Contributed paper

OPTO-ELECTRONICS REVIEW **12**(2), 199–112 (2004)

Crystal growth of the oxide fiber single crystal for optical applications

D.H. YOON*

Department of Advanced Materials Engineering, Sungkyunkwan University,
440-746 Suwon, Korea

Recently, certain materials have attracted attention for a new generation of high speed, efficient, multi-functional optical devices. Among these materials, small-diameter and long-length bulk crystals are of considerable interest for miniaturization and high efficiency. In particular, rod or fiber-like micro-single crystals have already received attention as attractive materials for a variety of electro-optical application, such as second harmonic generation (SHG), micro-laser sources or optical memory arrangements because of their extended interaction length and high optical intensity.

Keywords: optical application, micro-pulling down method, oxide crystals, crystal growth.

1. Introduction

Recently, certain materials have attracted attention for a new generation of high speed, efficient, multi-functional optical devices. Among these materials, small-diameter long-length bulk crystals are of considerable interest for miniaturization and high efficiency. In particular, fiber single crystals have already received attention as attractive materials for a variety of electro-optical application [1–3] because of their extended interaction length and high optical intensity.

There is increasing interest in the growth of rod or fiber-like micro-single crystals, suitable for application in non-linear optical and electro-optical devices [1,2,4,5], such as second harmonic generation (SHG), micro-laser sources or optical memory arrangements. An improved efficiency can be expected because of the high surface-volume ratio, the long interaction length and the high crystal quality [6,7].

Fiber single crystals were grown by variously modified melt growth like the laser heated pedestal growth (LHPG) method [8–11], the drawing down method [12] and the micro-Czochralski (μ-CZ) method [13].

For micro-single crystals the habit is of special importance because the dimension of the cross section approaches the diameter of the stimulating laser mode. Therefore the correlation between surface morphology and growth parameters, like starting composition of the melt and temperature field, are of considerable interest for optimization of the SHG properties.

Potassium lithium niobate, $K_3Li_{2-x}Nb_{5+x}O_{15+2x}$ (KLN), has been recognized as a potentially useful material for optical application [14,15], both because it is remarkably stable under intense laser radiation, and because of its large electro and non-linear optical coefficients.

Lithium niobate, $LiNbO_3$ (LN), is a material that combines excellent electro-optic, acousto-optic and non-linear properties with the possibility of rare earth or transition metal doping. The material can be used in bulk or it is possible to prepare low-loss optical waveguides [16]. Especially, erbium, Er_2O_3 (Er) doped LN has been proposed as a very useful material for optical storage, optoelectronics, and waveguide devices [17]. The crystal can simultaneously emit the second harmonic light through quasi-phase matching [18] and green light through up-conversion at room temperature [19] with a combination of the nonlinear optical properties of LN and the spectral properties of Er. For such optical properties, Er:LN single crystals of high quality without sub-grain boundaries are generally required.

The past four decades have seen an explosive development of eutectic composite materials. Directionally solidified super-alloy metals were extensively investigated for structural applications at high temperatures, as in turbine blades. Many studies of eutectic solidification provided a basic understanding of characteristics of those materials and a classification of various shapes of microstructure [20–22].

However, KLN is difficult to grow due to the formation of crack and composition change by conventional crystal growth method [23,24]. Similarly, because the congruent composition is different from the stoichiometric composition, the LN of the composition which escaped from the

*e-mail: dhyoon@skku.edu

congruent composition is very difficult to be grown to a single crystal without defect, too [25]. Likewise, because of their high melting points, high strength at high temperatures, and resistance to oxidation, attention turned towards various ceramic eutectics [26,27] though difficulty in controlling the microstructure still prevented the formation of regular structure.

Consequently, in this study, KLN and LN single crystal with congruent or stoichiometric composition and eutectic fibers were grown by the LHPG technique or micro-pulling down (μ-PD) method which is advanced method of crystal growth. The characteristics of this method has a high pulling rate, a low thermal strain compared with other growth methods and it is possible to grow a crystal from incongruent melt composition [28].

2. Crystal growth method and principle

It has been reported for several years that the interface electric field influences solute partitioning leading to an electric field-dependent effective solute partition coefficient [29,30]. This is peculiar to the growth by the laser heated pedestal growth (LHPG) technique or micro-pulling down (μ-PD) method which accompanies a significantly high temperature gradient at the solid-liquid interface.

LHPG or μ-PD methods make it possible to explore these field effects by controllably changing the growth velocity V, and the temperature gradients in liquid G_L, and in the solid G_S near the interface over a wide range.

2.1. Laser heated pedestal growth (LHPG)

Among vertical floating zone techniques, the laser heated pedestal growth (LHPG) technique is the most promising solution for growing fibers for optical data storage.

Since LHPG is a specific application of zone melting, certain aspects are important for the interpretation of the observed phenomena [31]. In the single pass zone melting model, the concentration distribution of the element A along the fiber without diameter reduction $C_{SA}(z)$ can be described by a well-known formula as follows [32]

$$C_{Sa}(z) = C_{0A}[1-(1-k_{0A})\exp(k_{0A}/lz)], \qquad (1)$$

where the equilibrium segregation coefficient k_{0A} of the element A is constant, the zone length l is constant and the concentration distribution C_{0A} of the element A is constant in the source rod. During the LHPG zone melting process four different regions can be distinguished, Fig. 1.

The principle of LHPG is illustrated in Fig. 2. A CO_2 laser beam creates a molten zone on the top of the source rod. The seed crystal is dipped into the molten zone and slowly withdrawn, pulling the growing crystal from the melts.

Simultaneously, the source rod is pushed upwards into the molten zone so as to maintain its volume constant. Assuming mass conservation, the ratio V_s/V_p of the rate of feeding of the source rod V_s to the rate of pulling of the crystal V_p is given by

$$V_s/V_p = (D_f/D_s)^2(\rho_f/\rho_s), \qquad (2)$$

where D_f is the diameter of the growing crystal, D_s is the diameter of the source rod, ρ_f is the density of the crystal, and ρ_s is the bulk density of the source material.

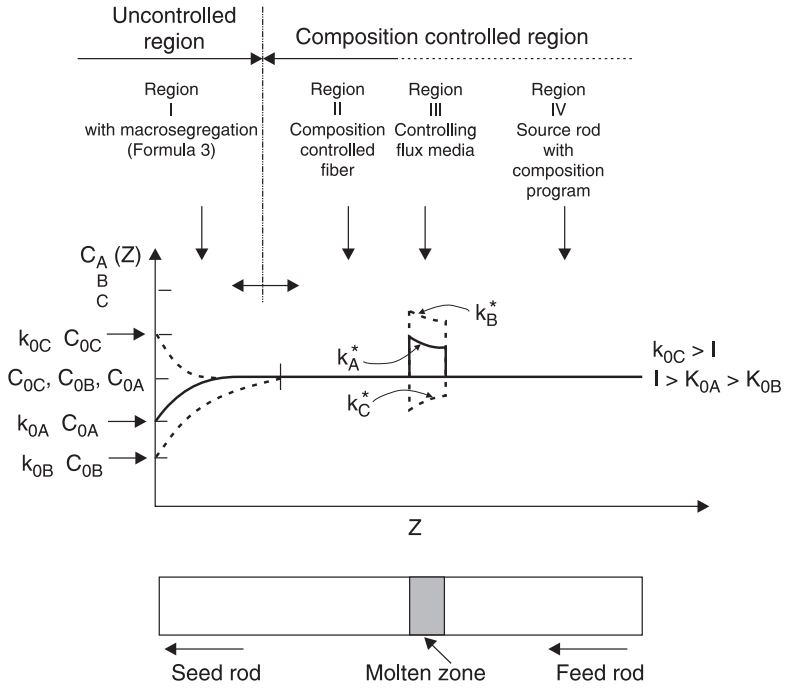

Fig. 1. Different composition regions along fiber crystal growth by the LHPG technique. The constant C_A, C_B, and C_C concentration in region I are slightly different from the C_A, C_B, and C_C concentration in region IV due to the control segregation effect (after Ref. 33).

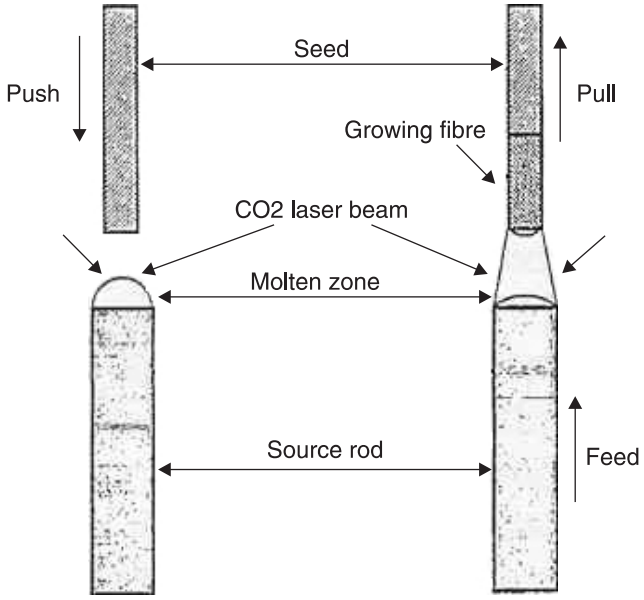

Fig. 2. A schematic diagram of LHPG method (after Ref. 34).

2.2. Micro-pulling down (μ-PD)

In the frame work of the "micro crystal project", since 1992, the development and broad application of single crystalline fiber growth by the "micro-pulling down (μ-PD)" method have been established at Fukuda Laboratory of Tohoku University [35]. The method, described for the first time by Yoon and Fukuda [36] and Yoon *et al*. [37–41] is used for the growth of oxide fiber single crystals.

The crystal growth method, called the μ-PD method, involves growing single crystals through a micro-nozzle by pulling in the downward direction, as shown in Fig. 3. This growth equipment consists of a crucible directly heated resistively, an after-heater made from Pt wire, an annealing

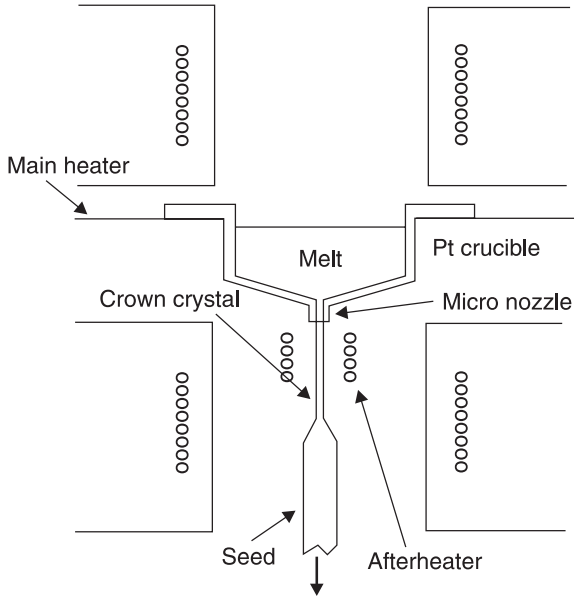

Fig. 3. Schematic diagram of the μ-PD apparatus (after Ref. 41).

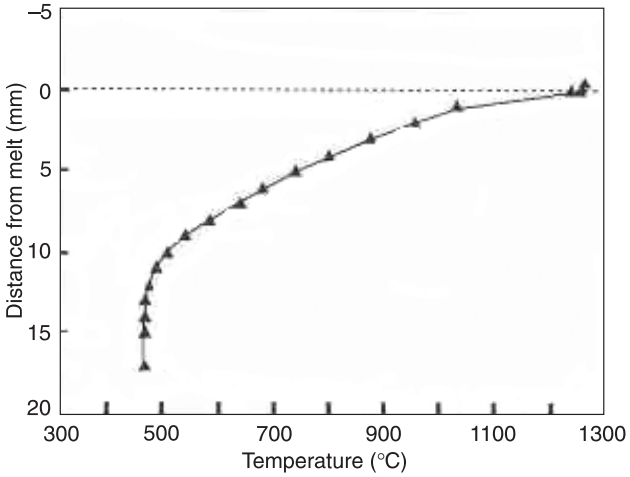

Fig. 4. Measured temperature distribution along the pulling axis (after Ref. 41).

furnace, and a crystal lowering mechanism containing a micro *X-Y* stage.

Figure 4 represents the temperature distribution measured by using a thermocouple along the pulling axis during the crystal growth. In the growth of the LN single crystals by the μ-PD method, *s* solid-liquid interface is established with a meniscus of narrow width (< 30 μm) and the same diameter as the crystal under the micro-nozzle. The axial temperature gradient at the solid-liquid interface was about 300°C/mm and was controlled by the temperature of the Pt after-heater (Fig. 3). The raw materials were melted within the Pt crucible and allowed to pass through the micro-nozzle. The single crystal was formed by attaching the seed crystal to the tip of the micro-nozzle and slowly pulling it downward with a constant velocity.

The alignment of the seed and the micro-nozzle was controlled by the micro *X-Y* stage. The crystals were grown in air atmosphere. The growth rate was varied from 12 to 90 mm/h. The configuration of the micro-nozzle and after-heater makes it easy to control the liquid-solid interface temperature and the crystal diameter. In this way, the growth conditions can be kept constant and it is reasonable to assume that it is possible to continue growing until the melt is all consumed.

One of the greatest advantages of the μ-PD method is the very high growth rate. Because of the absence of natural convection in a very thin nozzle, a diffusion-controlled regime with high composition homogeneity is created. Moreover, the temperature gradient along the growth axis near the nozzle is about 300°C/mm, enabling growth rates much faster than the Czochralski (CZ) method.

There are several basic parameters involved in crystal growth by the μ-PD technique:

- conservation of mass at the boundary between the capillary pipe and the molten zone,
- conservation of energy represented by the heat of fusion, the temperature conductivity of solid and liquid,
- mechanical stability of the molten zone shape represented by an interfacial wetting angle [42].

The μ-PD method has a specific advantage to the analysis of solute transport that since the free surface area is very limited and the height of free surface is 25–50 μm in most cases of this study, there is a little effect of Marangoni convection, Benard convection and buoyancy-driven convection [43]. In the coordinate system, tied to the moving interface, the flux J^j for the j^{th} species in the liquid is given by

$$J^j = -J^j(\partial C^j/\partial z) - VC^j + \\ + D^j z^j e[(E_c + E_t)C^j]/k_B T, \quad (3)$$

where the D^j is the diffusion constant and z^j is the valence of the j^{th} species, and k_B is the Boltzmann's constant.

The field-modified effective partition coefficient k_E^j is given by replacing k_0^j by k_{E0}^j and V by V_{EL}^j in the BPS equation

$$k_E^j = k_{E0}^j/\{k_{E0}^j + (1 - k_{E0}^j)\exp[-V_{EL}^j \delta_C / D_L^j]\}. \quad (4)$$

For each k_{E0}, there is the critical velocity V^*, which is represented by the intercept of the V-axis with the asymptotic line. That is, the effective velocity V_{EL} becomes 0 when the growth velocity V is equal to the critical velocity V^*

$$V^* = 2D_L \delta_C z_L e\alpha_L G_L/(D_L z_L e\alpha_i - 2_C k_B T), \quad (5)$$

V^* moves toward the $V = 0$ origin as G_L decreases, and it is very small and practically negligible when the temperature gradient is low, which is the case with the normal CZ growth. However, V^* becomes very important for the crystal growth by μ-PD technique which accompanies very high-temperature gradient at the interface. One should note that k_{E0} changes its sign from negative to positive at $V = V^*$. One should also note that a specific V^* for each ionic solute as there is a specific k_{E0} for them.

Solute conservation in a coordinate system moving at the velocity V is generally given by

$$-\partial J_\beta^j/\partial z = -\partial C_\beta^j/\partial t = D_\beta^j(\partial^2 C_\beta^j/\partial z^2) + (\partial/\partial z) \times \\ \{[V - (D_\beta^j z^j eE/k_B T) - u(z)]C_\beta^j\} \quad \beta = S, L \quad (6)$$

where $u(z)$ is the convection term which may be neglected in a simple no-mixing model which is the case with μ-PD method.

3. Fiber materials and their applications

3.1. Potassium lithium niobate

Potassium lithium niobate (KLN) is as a potentially useful material for non-linear optical applications [14] because it is remarkably stable to intense laser radiation and has excellent electro-optic and non-linear coefficients. KLN crystals double the frequency in the wavelength range from 790 nm to 920 nm by second harmonic generation (SHG) which takes place at room temperature which enables non-critical phase matching [44]. Recently, there has been a marked improvement in the efficiency of compact diode-pumped solid-state laser sources.

The most favourable compositions, including the tetragonal phase of KLN crystals, and suitable for non-linear optical effects, range between $0.1 \le x \le 0.5$. It can be seen from the phase diagram that the segregation effect between liquidus and solidus requires melt compositions with somewhat lower Nb_2O_5 content than in the desired solid phase.

KLN micro single crystals were grown by the micro-pulling down method in air. Starting compositions of $K_3Li_{2-x}Nb_{5+x}O_{15+2x}$ were used with $-0.3 < x < 0.3$. Growth orientations along the *a*-axis and *c*-axis ([100] and [001] direction, respectively, have been selected.

The grown KLN crystals with diameters of about 500 μm are free of cracks shown in Fig. 5. Good control of the crystal diameter is dependent on the melt composition. In fact, very good control of the crystal diameter at melt compositions $x \ge -0.3$ (at high Nb concentration, Nb ≥ 47 mol% in K:Li:Nb ratio) has been demonstrated. However,

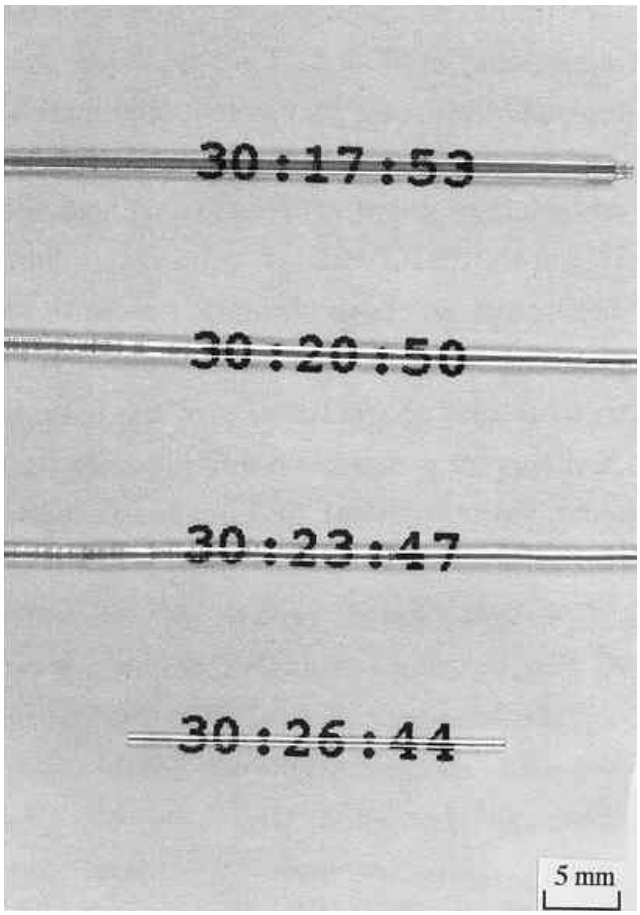

Fig. 5. Photograph of KLN micro-single crystals grown along the *a*-axis with a growth rate of 6 mm/h and various melt composition K:Li:Nb ratio (after Ref. 38).

at low Nb content ($x = -0.6$) the diameter drops drastically and changes uncontrollably.

The crystals show very uniform shapes and are free of cracks independent of the melt composition and the above-mentioned growth axis. The growth rate was 20 mm/h for crystals with diameter of 300 and 500 μm and 80 mm/h for that with a diameter of 150 μm. No fractures normal to the *c*-axis as in Kyropoulos [45] and Czochralski (CZ) [23] crystals have been observed. Also, the concentration in the solid was similar to that in the melt along the entire solidified fractions.

The etched cross sections of KLN micro-single crystal grown with a pulling down rate of 10 mm/h with a diameter of 500 μm are shown in Fig. 6. From these opposite-etched structures it can be readily seen that the KLN micro-single crystal grown by μ-PD method has a single domain structure.

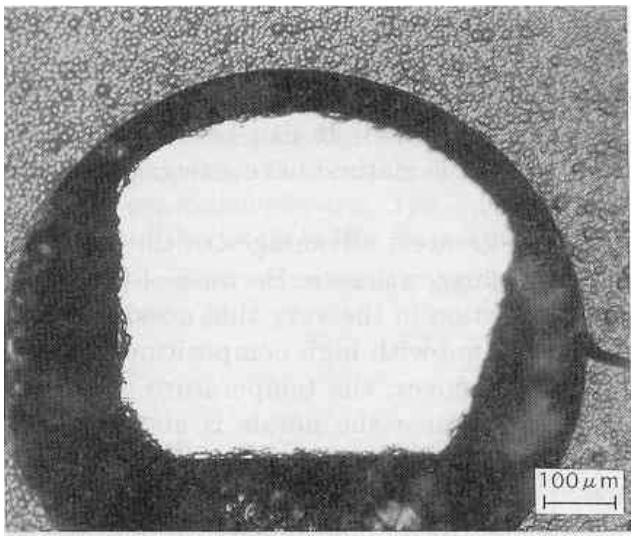

(a)

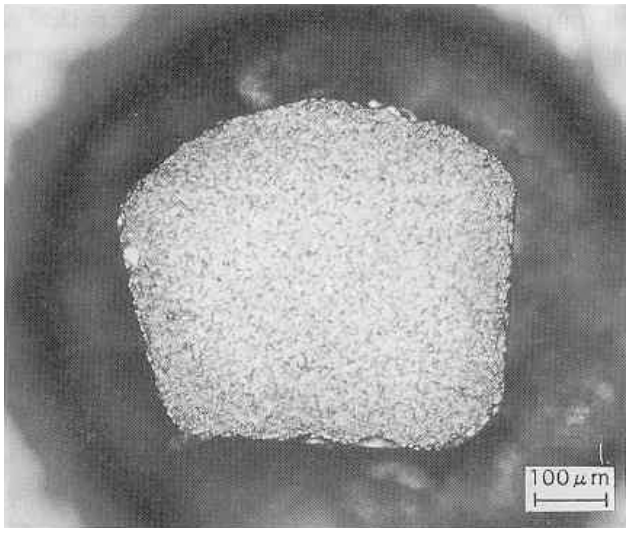

(b)

Fig. 6. The single domain structures of the *c*-axis KLN micro-single crystal: (a) positive plane and (b) negative plane (after Ref. 6).

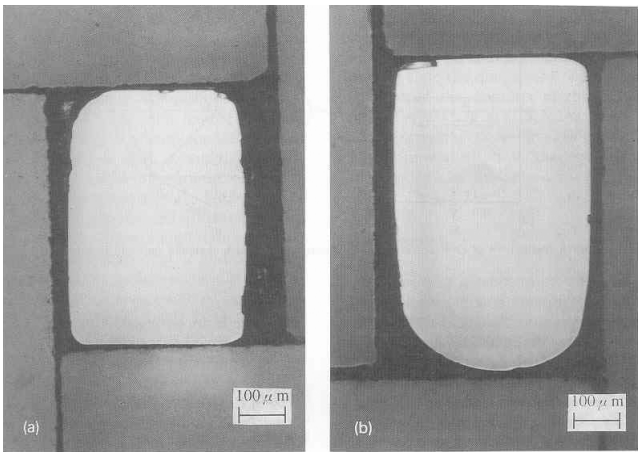

Fig. 7. Cross-section of *a*-oriented crystals: (a) rectangular ($x = -0.3$), (b) with rounded segment ($x = -0.3$) (after Ref. 39).

Figures 7 and 8 show the cross-sections of four different as-grown KLN crystals in pairs oriented along the *a*- and *c*-axis, respectively. The flatness of the prepared surfaces normal to the *a*-axis (important for the laser beam coupling) was of high quality, as was demonstrated by the interferometric fringe pattern [6]. For seed orientations parallel to one of the *a*-axis (of most interest for SHG device [14]), a nearly rectangular area, elongated along the *c*-axis, was formed [Figs. 7(a) and (b)]. In comparison, *c*-oriented growth was mostly characterized by a polygonal cross-section [Figs. 8(a) and (b)]. Only in one case was a near rectangular geometry observed. However, a strong dependence of the cross-section morphology on the starting melt composition has not been found using the μ-PD method.

Further, the overlapping between the symmetries of the crystal orientation and growth conditions needs to be considered. Figure 9 shows the idealized growth symmetries for *a*- and *c*-orientations. The point symmetry of $K_3Li_{2-x}Nb_{5+x}O_{15+2x}$ in the tetragonal region is 4/mm at

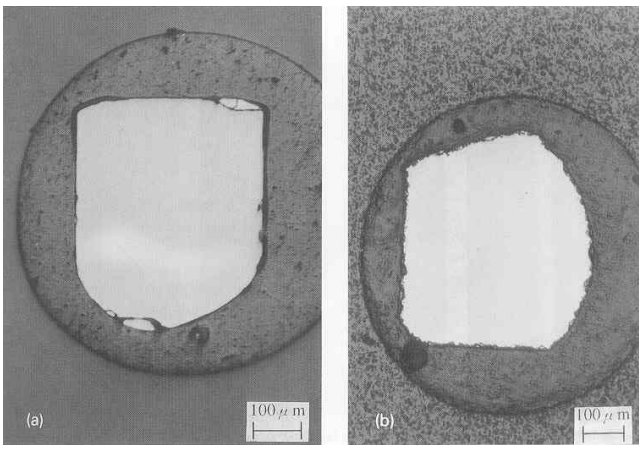

Fig. 8. Cross-section of *c*-oriented crystals: (a) nearly rectangular with rounded segment ($x = -0.3$) and (b) polygonal ($x = -0.3$) (after Ref. 39).

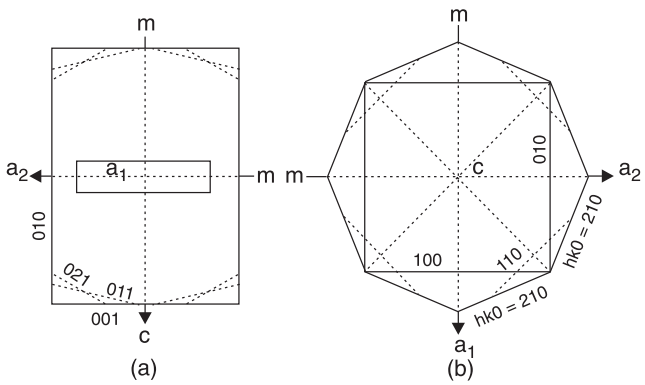

Fig. 9. Idealized growth symmetries of cross-sections: (a) *a*-oriented crystal with sketched unit cell in the centre and (b) *c*-oriented crystals (after Ref. 39).

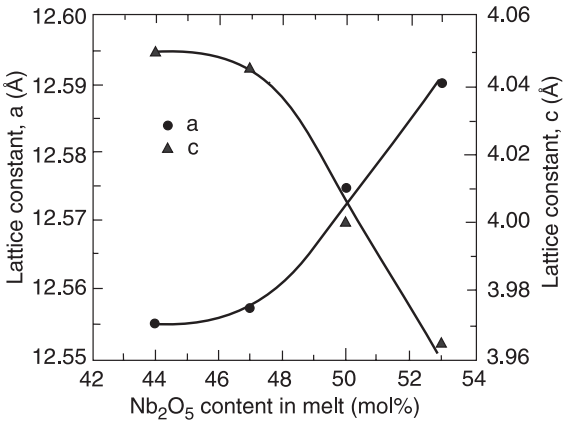

Fig. 11. Lattice constants *a* and *c* of grown crystals dependent on the melt compositions (after Ref. 38).

growth temperature. It is well known that at orientation parallel to the *c*-axis, this modification may tend to form ditetragonal prisms with eight identical {*hk*0} faces (usually {210}) parallel to [001] resembles an ordinary tetragonal prism [46].

Figure 10 shows the surfaces of as-grown KLN crystals along the *c* and *a*-axis in dependence on the melt composition. The surface of *c*-oriented crystals, grown from a melt with $x = 0$, shows mostly rounding segment [Fig. 10(a)]. Very flat (001) facets appear in the case of *a*-orientation at the composition of $x = 0.3$ [Fig. 10(b)]. However, this flatness roughens if the melt composition decreases below $x < 0.3$, as shown Fig. 8(c). Only a thin trace of the former large (001) faces was left [Fig. 10(c)]. As it can be seen, typical growth striations are created [47].

The lattice constants *a* and *c*, shown in Fig. 11, depend on the melt composition and change in $K_3Li_{2-x}Nb_{5+x}O_{15+2x}$ in between $-0.6 \le x \le 0.3$ from 12.555 Å and 4.050 Å to 12.590 Å and 3.965 Å, respectively. Whereas in *a*-oriented crystals with high Nb content ($x \ge -0.3$) a sensitive change with composition was detected, at low Nb concentration ($x \le -0.3$) the lattice constant was markedly uniform and relatively independent of the variation of the composition of the melt.

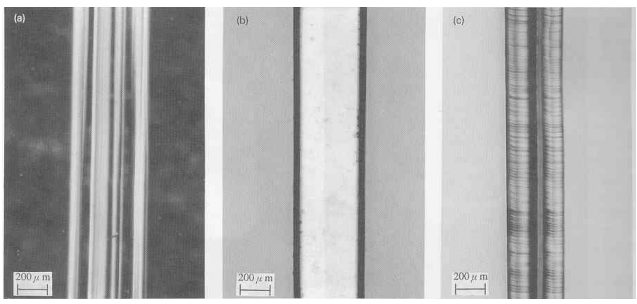

Fig. 10. Surface morphologies of as-grown KLN micro-crystals: (a) $x = 0$, *c*-orientation, view on *a*-plane, (b) $x = 0.3$, *a*-orientation, view on *c*-plane, (c) $x = -0.3$, *a*-orientation, view on *c*-plane (after Ref. 39).

Figure 12 shows the phase matched wavelength along the crystal length for μ-PD KLN crystals grown from melt compositions of $x = -0.6$ and -0.3. The wavelength variations are ±3 and ±2 nm, respectively.

We estimate that wavelength variations in KLN are above ±20 nm within the solidified fraction $g \le 0.1$, because of composition changes along the growth axis of 2 mol% in this region for a conventional growth method [49]. In μ-PD crystals, compositional homogeneity results in a nearly constant phase matched SHG wavelength along growth direction.

These results provide the dependence of the most appropriate composition for SHG applications from ultra-violet to green region and the developments of future growth technologies for a new material having improved composition homogeneity from incongruent melt compositions. It is considered that a change of composition in KLN crystals can affect the electro and non-linear optical properties because of the considerable change of the birefringence with variation of the Nb content. However, the SHG wavelength in μ-PD KLN crystals is not always proportional to the Nb content of the melt composition.

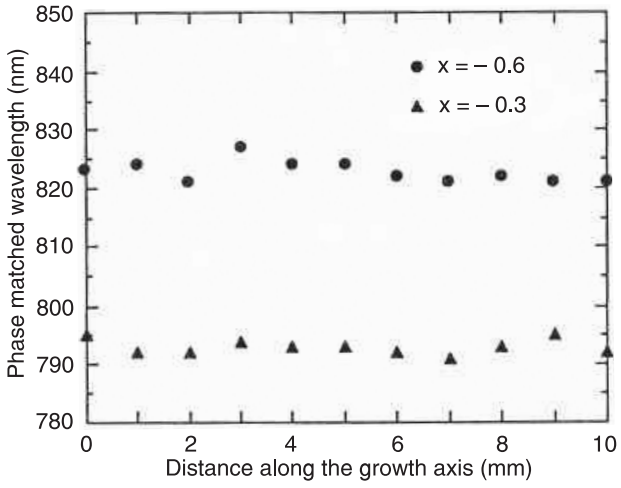

Fig. 12. Non-critical phase matched wavelength along the crystal length (after Ref. 48).

3.2. Lithium niobate (LN)

Lithium niobate (LN) is a useful material for non-linear optical applications because of its large non-linear optical coefficient and numerous favourable physical properties. For optical applications, LN single crystals of high quality without sub-grain boundaries are generally required.

LN single crystals, grown from a congruent melt, have been widely used in electro-optical applications. Two of the most practical problems of such crystals are DC drift and optical damage, the latter of which is known to be influenced by the photorefractive effect [50]. The photorefractive effect is composition sensitive. Although it is known that the compositions close to stoichiometry are obtained when the Li_2O rich liquid is used, homogeneous LN single crystals cannot be easily grown from the melts with more than 48.6 mol% Li_2O content by the conventional Czochralski (CZ) method because of the segregation effect [51]. Thus, the CZ LN crystals of nearly stoichiometric composition are not uniform against the optical damage. Also, multi-domain generation, growth ridges and structural defects adversely affect the quality of the conventional CZ crystals of as-grown state [52,53]. To overcome these problems of CZ, crystals were grown by laser heated pedestal growth (LHPG) method by Luh *et al*. who could obtain single-domain ones [54]. In order to establish an alternative way to obtain LN crystals free from the above-listed difficulties, we have investigated the growth of micro-single crystals by the micro-pulling down method, which promises a good control of shape and segregation [41].

Using the μ-PD method, LN single crystals of 60 to 800 μm in diameter were grown along the *x*-axis, *y*-axis, and *z*-axis, respectively. Figure 13 shows typical as-grown LN crystals which are represented with microscopic detail magnification of crystals with 60 to 300 μm diameter grown along the *x*-axis. We have grown crack-free *x*-oriented LN crystals with a length up to 10 cm and high diameter constancy using the μ-PD method. An aspect ratio of the crystal length to the crystal diameter of about 200 has been obtained. Homogeneous colourlessness over the whole length and uniform diameter independent of the growth directions can be shown. Also, the crystals grown were free of cracks from the various compositions of the melt having congruent (48.6 mol% Li_2O), and stoichiometry (50 or 58 mol% Li_2O) until the *g* value (solidification ratio of melt) was about 1.

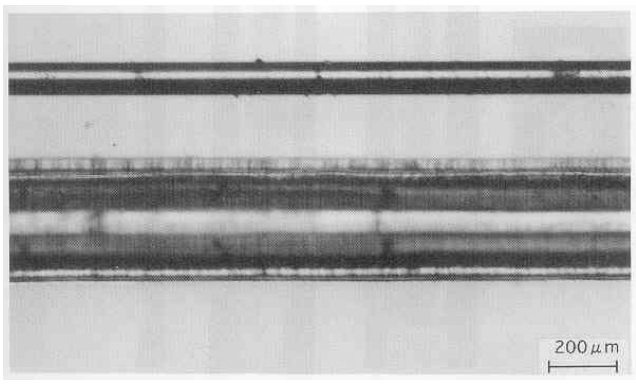

Fig. 13. Microscopic photograph LN micro-single crystals grown along the *x*-axis from 48.6 mol% Li_2O with diameters of 60 and 300 μm, respectively (after Ref. 40).

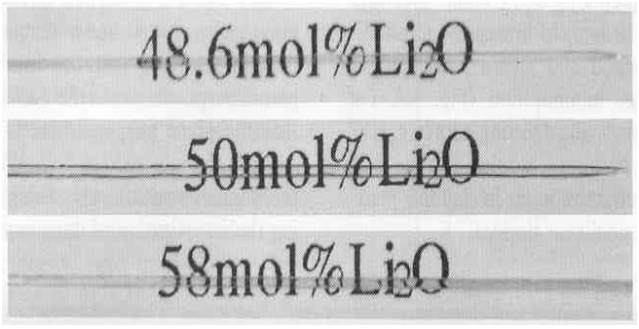

Fig. 14. Photograph of *x*-oriented LN micro-single crystals with diameters of 500 μm grown from melts with 48.6, 50, and 58 mol% Li_2O (after Ref. 37).

Figure 14 shows typical *x*-oriented LN micro-single crystals with diameters of 500 μm, grown by the μ-PD method from the melt compositions with 48.6, 50, and 58 mol% Li_2O contents, respectively.

The morphology of the micro-crystals depended on the growth direction very sensitively. Typical growth ridges with a width of about 50 μm, elongated along the growth axis, were observed on the crystal surface. They reflect the 2-fold symmetry of *x*- or *y*-orientation or 3-fold symmetry of *z*-orientation, respectively, and are positioned similarly to CZ crystals [53]. Figure 15(a) shows the cross section of an *x*-oriented crystal with a characteristic 2-fold symmetry. In Figs. 15(b) and 15(c), the morphology of growth ridges of two crystals, grown under different conditions, is compared. It can be seen that the ridge width increases when the temperature gradient decreases from 200 to 300°C/mm at the same growth rate (60 mm/h). The size ratio (ridge width to crystal diameter) is markedly larger in uncontrolled micro-single crystals.

Dislocations in a micro-single crystal were studied by X-ray topography. Figures 16(a,b,c) are topographic images obtained from each sample under different diffraction conditions as attached. Here, as shown in Fig. 16(d) for comparison, many dislocations and sub-grain boundaries are observed obviously in a LN wafer grown by the conventional CZ method. Contrarily, dislocations and sub-grain boundaries cannot be detected in the μ-PD crystal. The etch pits reveal the point of intersection of dislocations with the surface.

Figure 17 is a photograph of the etched surface seen the *y*-face of an *a*-axis grown LN micro-single crystal. We could not detected the dislocation etch pit which is consistent with that of X-ray topograph.

It is well known that dislocations are a direct result of thermal stresses. Usually, in conventional crystals the ideal stress-free state cannot be realized because of the presence

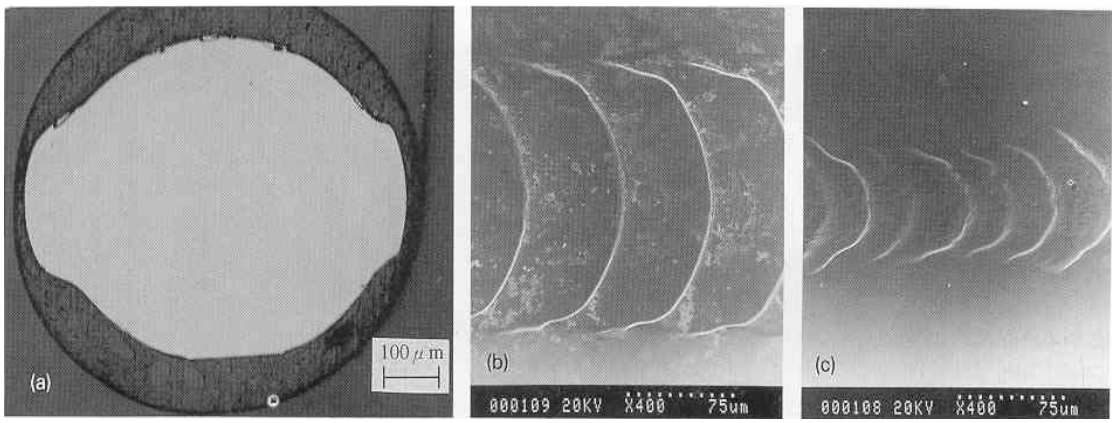

Fig. 15. Morphology of *x*-oriented LN micro-single crystal at a pulling rate of 60 mm/min: (a) typical cross section at a temperature gradient of 200°C/mm, (b) growth ridges observed on the crystal grown under the same conditions as in case (a), (c) growth ridges on the crystal grown under a temperature gradient of 300°C/mm (after Ref. 37).

of non-linear temperature gradient [55]. Also, a correlation to the crystal diameter has been discussed [56].

However, the present results grown by the μ-PD method show a dislocation-free single crystal empirically.

The erbium (Er) doped fibers were used to prove the physical mechanism of two-photon as well as excited-state absorption under near-infrared (NIR) diode laser excitation [57–59] and room temperature green up-conversion lasers were developed by pumping Er-doped fibers with infrared (IR) lasers [60–62]. The doping of LN is an interesting task because it enables us the combination of the optically active Er^{3+} ions with the excellent nonlinear, electro-optical and acousto-optical properties of this material [63]. Then, the Er:LN has been proposed as a very useful material for optical storage, optoelectronics, and waveguide devices [64].

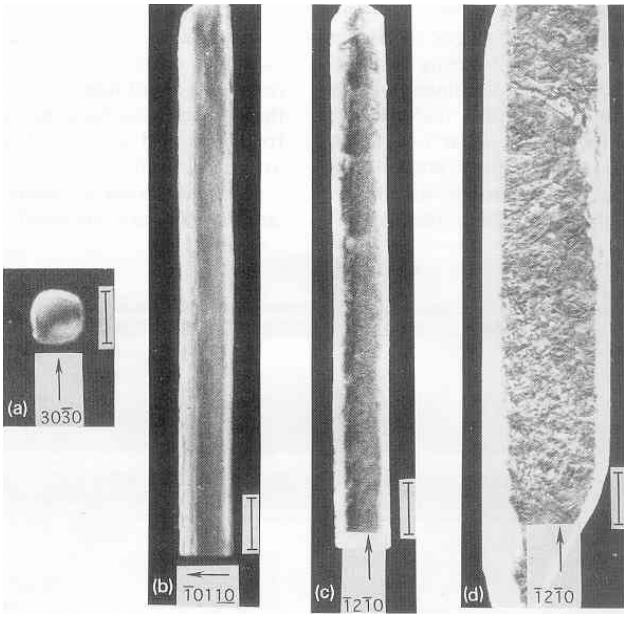

Fig. 16. X-ray topographs of LN single crystal of (a) perpendicular and (b)-(d) parallel planes along the *x*-axis taken from different diffraction plane as attached: (a), (b), and (c) μ-PD crystal, (d) CZ crystal (Marker represents 500 μm) (after Ref. 41).

Therefore, the Er doped LN single crystal fibers with congruent and stoichiometric composition were grown by μ-PD method. The crystals were transparent, but the colours of grown crystals were changed from colourless to pink (in congruent composition) and orange (in stoichiometric composition) depending on increase in the Er^{3+} concentration in the crystal.

The concentration of Er^{3+} ions was distributed homogeneously along the growth axis [65]. This is probably because the nature convection was restricted in the micro-nozzle and the Er constituent became unified along the growth axis.

Figure 18 shows the up-conversion intensity measured in congruent Er:LN single crystal fibers. It means that the Er:LN possesses strong up-conversion emission, at the green wavelength region of 540–560 nm. The dominant peaks of up-conversion intensities around 550 nm were due to the $^4S_{3/2} \rightarrow {}^4I_{15/2}$ transition, while the small peaks around 530 nm were due to the $^2H_{11/2} \rightarrow {}^4I_{15/2}$ transition [67]. For the same pump intensities, the measured up-conversion intensity for the 3 mol% Er doped crystals was about 3.5 times larger than that of the 1 mol% Er doped crystals. It shows that intensities of up-conversion are increased in proportion to increase of Er^{3+} concentration.

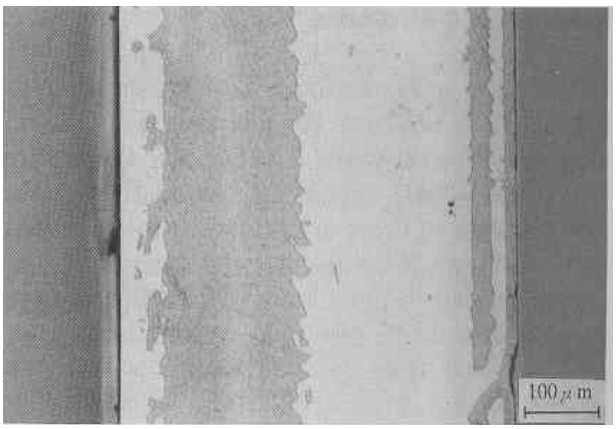

Fig. 17. Etched surface seen on *y*-face of an *a*-axis grown crystal (after Ref. 41).

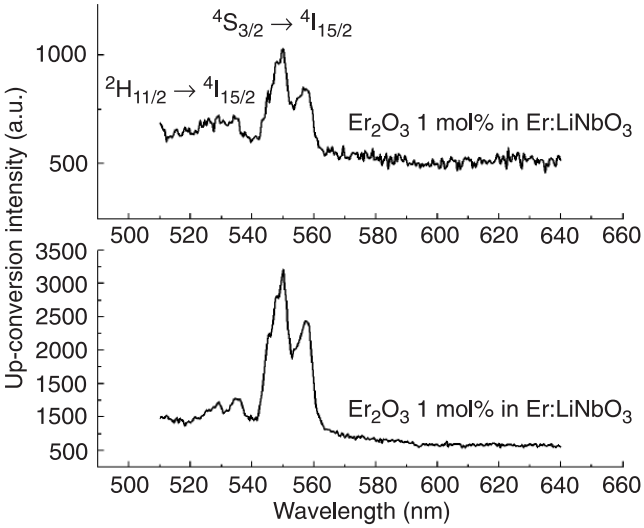

Fig. 18. The up-conversion intensity of congruent Er:LN single crystals: (a) 1 mol% Er doped and (b) 3 mol% Er doped crystals (after Ref. 66).

Figure 19 shows the up-conversion intensity of stoichiometric LN single crystal doped with 1 mol% Er. Similarly, the stoichiometric LN has the strongest peak intensity around 550 nm wavelength region. The measured up-conversion intensity of 1 mol% Er doped stoichiometric LN single crystal was about 2 times higher than that of 3 mol% Er doped congruent LN single crystal and the intensity was increased with the adding of Er concentration. It means that the stoichiometric LN single crystal is desirable in comparison with congruent LN.

Zhong *et al*. showed that LN doped with about 5% or more magnesium oxide, MgO (Mg) exhibits a remarkably reduced photo-refractive response compared with undoped $LiNbO_3$ [68].

Also, Er:Mg:LN crystal fibers were grown by the μ-PD method from a congruent melt. The grown crystals are transparent and crack-free and have a light yellow colour which is characteristic of Mg doping. The segregation coefficient

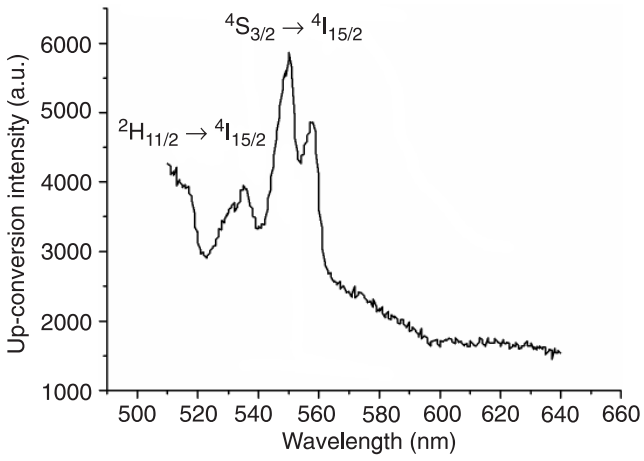

Fig. 19. Up-conversion intensity of stoichiometric LN crystal doped with 1 mol% Er (after Ref. 66).

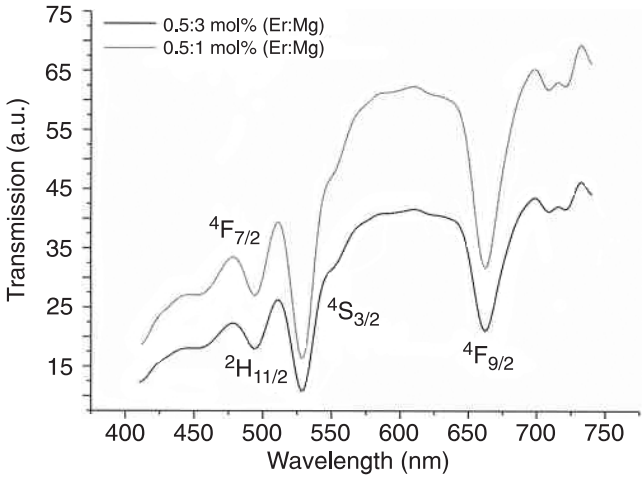

Fig. 20. Transmission spectrum of Er and Mg co-doped stoichiometric LN single crystals (after Ref. 69).

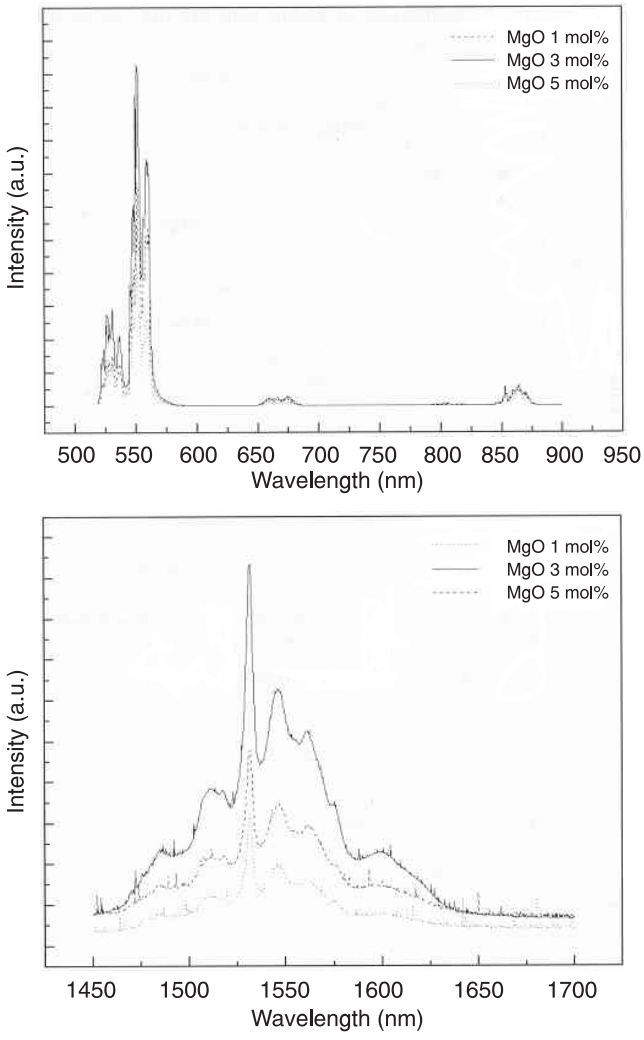

Fig. 21. Photoluminescence (PL) spectra of the Er^{3+} ion doped in the Mg:LN (after Ref. 72).

of Er^{3+} ions was in the range of 0.85–0.86 according to the Mg concentration in the starting charge. So, the segregation coefficient of Mg ions was about 1.02 according to Mg concentrations in the melt. It can be explained with a view of growth method because the nature convection was restricted in the micro-nozzle and the Er and Mg constituent in Er:Mg:LN melt became unity along the growth axis leading to the homogeneous composition throughout the crystal.

The transmission spectra at a room temperature are shown in Fig. 20. Several energy bands are observed in the grown crystals [70]. The observed energy bands are due to the f^{11} electronic configuration of Er^{3+}, it is the transition from the ground state $^4I_{15/2}$ to the excited states which are created from the $4f^{11}$ electron configuration [71]. Also, the transmission spectra is similar to those observed in Mg 1 mol% doped crystal containing Er^{3+} ions, but relative absorption was different. From a viewpoint of reducing the photo-refractive effect, relative absorption spectrum according to Mg content, the Er:Mg:LN crystal grown with added Mg of 3 mol% was observed the progressive photo-refractive resistance more than grown crystal from 1 mol% Mg and 0.6 mol% Er co-doped LN congruent melt.

The spectra of crystal fibers have shown an energy band emission spectrum with the strongest line corresponding to the $^4S_{3/2} \rightarrow {}^4I_{15/2}$ transition, as observed around the UV, NIR regions under the 514 nm excitation (Fig. 21). The emission intensity for the 3 mol% Mg doped crystals was about 1 time larger than that for the 1 and 5 mol% Mg doped crystals.

4. Eutectics

In various industrial fields, there is a great need for materials having high strength combined with high toughness at high temperature. In this regard, many monolithic and composite materials such as directionally solidified ceramic eutectics are attracting considerable interest because of their high structural stability up to nearly the melting temperature [73]. In the early 1960s, systematic investigations of ceramic eutectics began and a considerable number of researches have been devoted to the structure and properties of these eutectics.

A few years ago, new and good experimental results were reported for Al_2O_3-based eutectic systems such as $Al_2O_3/GdAlO_3$ [73] and Al_2O_3/YAG [74–77]. Especially, growth of these materials in fiber form yields an improvement in the mechanical properties [77] because fiber crystals have a very high strength due to their crystalline perfection and small cross-sections. On the other hand, Al_2O_3/ZrO_2 eutectic crystal systems are also of interest for high strength applications. The solidification of the Al_2O_3/ZrO_2 and Y_2O_3-doped Al_2O_3/ZrO_2 eutectic system has been studied previously [78–82].

Recently, Lee *et al*. [83] investigated micro-structural changes of Al_2O_3/ZrO_2 eutectic fibers as a function of solidification rate by micro-pulling down (μ-PD) method

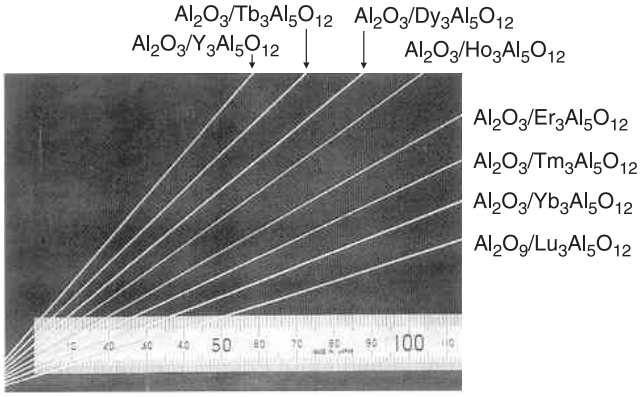

Fig. 22. $Al_2O_3/RE_3Al_5O_{12}$ (RE = Tb-Lu, Y) eutectic fibers (after Ref. 87).

which has been demonstrated to be an effective technique for the growth of fiber crystals [76,84–86], and the eutectic fibers were grown by the μ-PD method.

Figure 22 shows the Al_2O_3/Garnet system eutectic fibers obtained. In this system, reasonably stable growth was achieved over a wide range of pulling rates, 0.1–20 mm/min, with the highest achievable pulling rate being around 30 mm/min. The diameter of these fibers was well controlled in the range from 200 to 500 μm, and the length was 550 mm. The fibers were white or coloured, depending on the rare-earth ion.

The lamellar thickness of the zirconia, ZrO_2 (Zr) phase was found to be uniform for each cross-section investigated and decreased from 380 to 110 nm as the pulling rate increased from 1 to 15 mm/min as plotted comparatively with $Al_2O_3/Y_3Al_5O_{12}$ in Fig. 23.

The general relation $\lambda \sim v^{-1/2}$ where λ is the inter-lamellar spacing and v is the solidification rate, can also be applied to the lamellar structure of Al_2O_3/Zr eutectic. The proportional constant is close to 1, if λ has the dimension

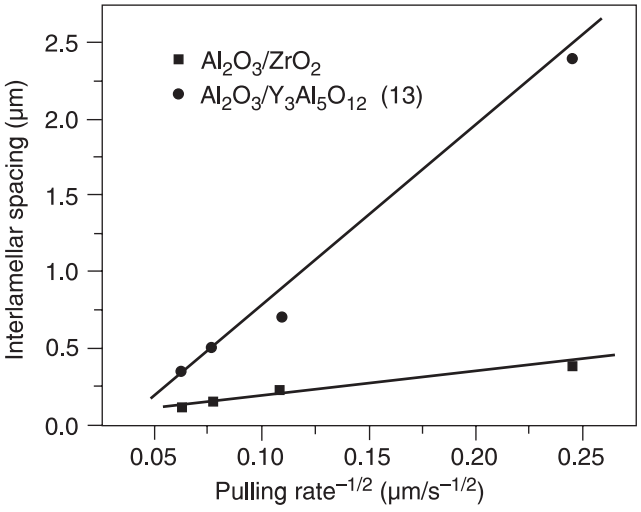

Fig. 23. Lamellar thickness of Zr phase in the matrix Al_2O_3 of versus pulling rate (after Ref. 83).

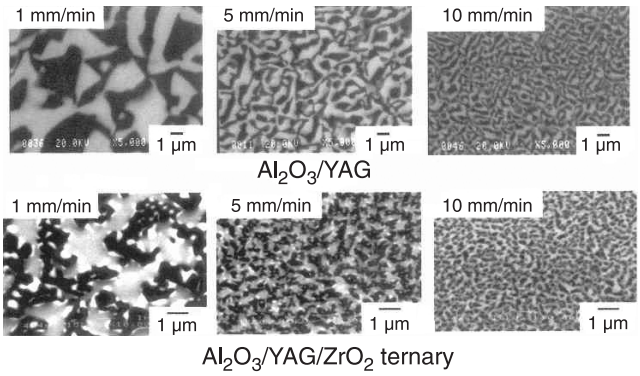

Fig. 24. SEM images of perpendicular cross-section of Al_2O_3/YAG binary and Al_2O_3/YAG/Zr ternary eutectic fibers grown at various pulling rates, 1, 5, and 10 mm/min (after Ref. 88).

in μm and v is in μm/s. This value is small relative to the value of 10 for $Al_2O_3/Y_3Al_5O_{12}$ and $Al_2O_3/GdAlO_3$ eutectic systems [86]. The nanometer scale of lamellar thickness is very thin compared to Al_2O_3/YAG eutectic fiber having micrometer-ordered lamellar thickness [85].

Typical eutectic microstructures were shown in Figs. 24 and 25 as a function of solidification rate. The eutectic microstructures were composed of two or three phases depending on the eutectic component, and distinguished by their different shapes and colours. The black matrix was shown to be Al_2O_3, and the white phases were YAG or Zr in binary systems. While the eutectics containing YAG showed homogeneous "Chinese script" lamellar pattern like Fig. 22, the microstructure of Al_2O_3/Zr binary eutectics changed from lamellar structure to cellular-lamellar pattern via circular and triangular colony structure with the solidification rate as shown in Fig. 25.

In the ternary eutectics, gray YAG phase made a homogeneous second phase on the black sapphire matrix, and the Zr phase as relatively small particles that appear white in the micrograph. Both YAG and Zr phases in the ternary eutectics showed different morphologies compared to those of respective Al_2O_3-based binary eutectic systems. It could be observed that neighbouring YAG grains were connected to each other, but the Zr particles were scattered.

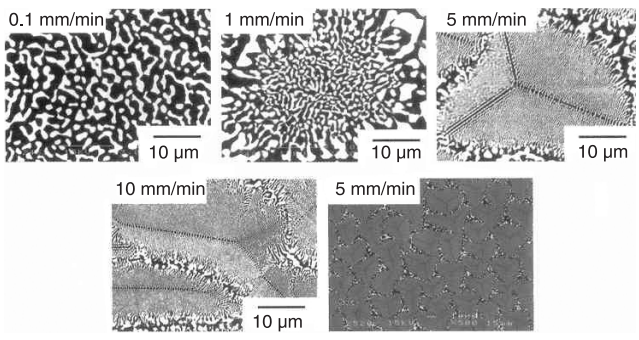

Fig. 25. SEM images of perpendicular cross-section of Al_2O_3/Zr (Y_2O_3) binary eutectic fibers grown at the pulling rate of 0.1, 1, 5, and 10 mm/min (after Ref. 88).

5. Conclusions

Among the materials for a new generation of high speed, efficient, multi-functional optical devices, small-diameter and long-length bulk crystals are of considerable interest for miniaturization and high efficiency. In particular, rod or fiber-like micro-single crystals have already received attention as attractive materials for a variety of electro-optical application, such as second harmonic generation (SHG), micro-laser sources or optical memory arrangements because of their extended interaction length and high optical intensity.

Because the dimension of the cross section approaches the diameter of the stimulating laser mode, the habit is of special importance for micro-single crystals. Therefore the correlation between surface morphology and growth parameters, like starting composition of the melt and temperature field, are of considerable interest for optimization of the SHG properties.

Consequently, the fiber crystals such as potassium lithium niobate (KLN), lithium niobate (LN) and eutectic were grown by variously modified melt growth like the laser heated pedestal growth (LHPG) technique or micro-pulling down (μ-PD) method which accompanies a significantly high temperature gradient at the solid-liquid interface. KLN is as a potentially useful material for non-linear optical applications because it is remarkably stable to intense laser radiation and has excellent electro-optic and non-linear coefficients. Similarly, LN is a useful material for non-linear optical applications because of its large non-linear optical coefficient and numerous favourable physical properties. The growth of eutectic materials in fiber form yields an improvement in the mechanical properties because fiber crystals have a very high strength due to their crystalline perfection and small cross-sections.

In case of LHPG technique, a CO_2 laser beam creates a molten zone on the top of the source rod, then the seed crystal is dipped into the molten zone and slowly withdrawn, pulling the growing crystal from the melts and the μ-PD method involves growing single crystals through a micro-nozzle by pulling in the downward direction. The LHPG or μ-PD methods make it possible to explore the field effects by controllably changing the growth velocity V, the temperature gradients in liquid G_L and in the solid G_S near the interface over a wide range.

In this study, the grown fiber crystals had no crack and sub-grain boundary and good optical properties and physical properties.

Of course, there are technological problems, the fiber crystal growth from the melt allows for excellent fundamental studies on nearly unidirectional heat and mass transports, growth kinetics, phase relations and diagrams, capillary stabilities and dynamics of individual imperfections. Especially, even before the costly conventional growth methods of bulk crystals are used, the brief and uncomplicated test of the crystallization behaviour of new materials by fiber growth is of immense encouragement for research.

References

1. S. Sudo, I. Yokohama, A. Cordova-Plaza, M.M. Fejer, and R.L. Byer, "Uniform refractive index cladding for $LiNbO_3$ single-crystal fibers", *Appl. Phys. Lett.* **56**, 19–31 (1990).
2. L. Hesselink and S. Redfield, "Photorefractive holographic recording in strontium barium niobate fibers", *Opt. Lett.* **13**, 877–879 (1988).
3. H. Yoshinaga and K. Kitayama, "Holographic image storage in iron-doped lithium niobate fibers", *Appl. Phys. Lett.* **56**, 1728–1730 (1990).
4. J. Stone, C.A. Burrus, and A.G. Dentai, "Nd:YAG single-crystal fiber laser: Room-temperature cw operation using a single LED as an end pump", *Appl. Phys. Lett.* **29**, 37–39 (1976).
5. D.H. Jundt, M.M. Fejer, and R.L. Byer, "Characterization of single-crystal sapphire fibers for optical power delivery systems", *Appl. Phys. Lett.* **55**, 2170–2172 (1989).
6. D.H. Yoon, M. Hashimoto, and T. Fukuda, "Growth and characterization of $K_3Li_{2-x}Nb_{5+x}O_{15+2x}$ micro single crystals formed by the μ-pulling down method for blue SHG applications", *Jap. J. Appl. Phys.* **33**, 3510–3513 (1994).
7. C.A. Burrus and J. Stone, "Room-temperature continuous operation of a ruby fiber laser", *J. Appl. Phys.* **49**, 3118–3123 (1978).
8. R.S. Feigelson, "Pulling optical fibers", *J. Crystal Growth* **79**, 669–680 (1986).
9. M.M. Fejer, J.L. Nightingale, G.A. Magel, and R.L. Byer, "Laser-heated miniature pedestal growth apparatus for single-crystal optical fibes", *Rev. Sci. Instr.* **55**, 1791–1796 (1984).
10. M. Saifi, B. Dubois, E.M. Vogel, and F.A. Thiel, "Growth of tetragonal $BaTiO_3$ single crystal fibers", *J. Mater. Res.* **1**, 452–456 (1986).
11. J.K. Yamamoto, S.A. Markgraf, and A.S. Bhalla, "$Sr_xBa_{1-x}Nb_2O_6$ single crystal fibers: dependence of crystal quality on growth parameters", *J. Crystal Growth* **123**, 423–435 (1992).
12. H. Oguri, H. Yamamoto, and T. Orito, "Growth of MgO doped $LiNbO_3$ single crystal fibers by a novel drawing down method", *J. Crystal Growth* **110**, 669–676 (1991).
13. N. Ohnishi and T. Yao, "A novel growth technique for single-crystal fibers: the micro-czochralski (μ-CZ) method", *Jap. J. Appl. Phys.* **28**, L278–L280 (1989).
14. L.G. Van Uitert, S. Singh, H.J. Levinstein, J.E. Geusic, and W.A. Bonner, "A new and stable nonlinear optical material", *Appl. Phys. Lett.* **11**, 161–163 (1967).
15. L.G. Van Uitert, H.J. Levinstein, J.J. Rubin, C.D. Capio, E.F. Dearborn, and W.A. Bonner, "Some characteristics of niobates having 'filled' tetragonal tungsten bronze-like structures", *Mat. Res. Bull.* **3**, 47–57 (1968).
16. B. Herreros and G. Lifante, "$LINBO_3$ optical wave-guides by Zn diffusion from vapour-phase", *Appl. Phys. Lett.* **66**, 1449–1451 (1995).
17. M. Tsuda, K. Inoue, S. Inoue, and A. Makishima, "Upconversion mechanism in Er^{3+}-doped fluorozirconate glasses under 800 nm excitation", *J. Appl. Phys.* **85**, 29–37 (1999).
18. V. Bermudez, J. Capmany, J. Garcia Sole, and E. Diehguez, "Growth and second harmonic generation characterization of Er^{3+} doped bulk periodically poled $LiNbO_3$", *Appl. Phys. Lett.* **73**, 593–595 (1998).
19. J. Zheng, Y. Lu, G. Luo, J. Ma, and Y. Lu, "Visible dual-wavelength light generation in optical superlattice Er:$LiNbO_3$ through upconversion and quasi-phase-matched frequency doubling", *Appl. Phys. Lett.* **72**, 1808–1810 (1998).
20. J. D. Hunt and K.A. Jackson, "Binary eutectic solidification", *Trans. Metall. Soc. AIME* **236**, 843–852 (1966).
21. R. Elliot, "Eutectic solidification", *Int. Met. Rev.* **22**, 161–186 (1977).
22. W. Kurz and D.J. Ficher, "Dendrite growth in eutectic alloys: the coupled zone", *Int. Met. Rev.* **24**, 177–204 (1979).
23. W.A. Bonner, W.H. Grodkiewicz, and L.G. Van Uitert, "The growth of $K_{0.6}Li_{0.4}NbO_3$ crystals for electro-optic and non-linear applications", *J. Crystal Growth* **1**, 318–319 (1967).
24. T. Fukuda, "Growth and crystallographic characteristics of $K_3Li_2Nb_5O_{15}$ single crystals", *Jap. J. Appl. Phys.* **8**, 122–129 (1969).
25. J.M. Ko, H. Cho, S.H. Kim, J.K. Choi, and K.H. Auh, "A study on the optical properties of LiNbO3 single crystal grown by floating zone method", *J. Kor. Ass. Crystal Growth* **5**, 318–331 (1995).
26. V.S. Stubican and R.C. Bradt, "Eutectic solidification in ceramic systems", *Annu. Rev. Mater. Sci.* **11**, 267–297 (1981).
27. J.D. Hunt and S.Z. Lu, *Handbook of Crystal Growth* **2**, 1111 (1994).
28. K. Imai, M. Imaeda, S. Uda, T. Taniuchi, and T. Fukuda, "Homogeneity and SHG properties of $K_3Li_{2-x}Nb_{5+x}O_{15+2x}$ single crystals grown by micro-pulling-down technique", *J. Cryst. Growth* **177**, 79–87 (1997).
29. S. Uda and W.A. Tiller, "The influence of an interface electric field on the distribution coefficient of chromium in $LiNbO_3$", *J. Crystal Growth* **121**, 93–110 (1992).
30. S. Uda and W.A. Tiller, "Cr migration associated with interface electric fields during transient $LiNbO_3$ crystal growth", *J. Crystal Growth* **126**, 396–412 (1993).
31. L. Galambos, S. Erdei, I. Tanaka, L. Hesselink, L.E. Cross, R.S. Feigelson, F.W. Ainger, and H. Kojima, "Inhomogeneities and segregation behaviour in strontium-barium niobate fibers grown by laser-heated pedestal growth technique", *J. Crystal Growth* **167**, 660–669 (1996).
32. W.G. Pfann, *Zone Melting*, Wiley, New York, 1966.
33. S. Erdei, L. Galambos, I. Tanaka, L. Hesselink, L.E. Cross, R.S. Feigelson, F.W. Ainger and H. Kojima, "Inhomogeneities and segregation behaviour in strontium–barium niobate fibers grown by laser-heated pedestal growth technique", *J. Crystal Growth* **167**, 670–680 (1996).
34. X. Qi, R. Illingworth, H.G. Gallagher, T.P.J. Han, and B. Henderson, "Potential laser gain media with the stoichiometric formula $RETiNbO_6$", *J. Crystal Growth* **160**, 111–118 (1996).
35. J.A. Burton, R.C. Prim, and W.P. Slichter, "The distribution of solute in crystals grown from the melt", *J. Chem. Phys.* **21**, 1987–1991 (1953).
36. P. Rudolph, "The virtues of Fukuda laboratory of crystal growth", *III-Vs Review*, *Elsevier* **9**, 27–32 (1996).
37. D.H. Yoon and T. Fukuda, "Characterization of $LiNbO_3$ micro single crystals grown by the micro-pulling-down method", *J. Crystal Growth* **144**, 201–206 (1994).
38. D.H. Yoon and T. Fukuda, "Compositional homogeneity of potassium lithium niobate crystals grown by micro pulling

down method", *J. Kor. Ass. Crystal Growth* **4**, 405–410 (1994).
39. D.H. Yoon, P. Rudolph, and T. Fukuda, "Morphological aspects of potassium lithium niobate crystals with acicular habit grown by the micro-pulling-down method", *J. Crystal Growth* **144**, 207–212 (1994).
40. D.H. Yoon, I. Yonenaga, and T. Fukuda, "Characterization of dislocations in a $LiNBO_3$ single-crystal grown by micro-pulling-down method", *Cryst. Res. Technol.* **29**, 1119–1122 (1994).
41. D.H. Yoon, I. Yonenaga, T. Fukuda, and N. Ohnishi, "Crystal growth of dislocation-free $LiNbO_3$ single crystals by micro pulling down method", *J. Crystal Growth* **142**, 339–343 (1994).
42. R.S. Feigelson, W.L. Kway, and R.K. Route, "Single-crystal fibers by the laser-heated pedestal growth method", *Opt. Eng.* **24**, 1102–1107 (1985).
43. S. Uda, J. Kon, K. Shimamura, and T. Fukuda, "Analysis of Ge distribution in $Si_{1-x}Ge_x$ single crystal fibers by the micro-pulling down method", *J. Crystal Growth* **167**, 64–73 (1996).
44. J.J.E. Reid, "Resonantly enhanced, frequency doubling of an 820 nm gaalas diode-laser in a potassium lithium-niobate crystal", *Appl. Phys. Lett.* **62**, 19–21 (1993).
45. T. Fukuda, H. Hirano, and S. Koide, "Growth and properties of ferroelectric $K_3Li_2(Ta_xNb_{1-x})_5O_{15}$", *J. Crystal Growth* **6**, 293–296 (1970).
46. F.D. Bloss, *Crystallography and Crystal Chemistry*, Holt, Rinehart and Winston, New York, 1971.
47. A.A. Chernov, *Modern Crystallography*, Springer Series in Solid-State Sciences, Vol. 36, Springer, Berlin, 1984.
48. D.H. Yoon and T. Fukuda, "Second harmonic generation (SHG) properties of potassium lithium niobate crystals grown by Mu-PD method", *J. Kor. Ass. Crystal Growth* **5**, 94–99 (1995).
49. D.H. Yoon, N. Shimo, M. Hashimoto, Y. Okano, T. Sasaki, and T. Fukuda, "Growth of non-linear optical $K_3Li_{2-x}Nb_{5+x}O_{15}$ single crystal from the incongruent solution", *The 37th Discussion Meeting of Synthetic Crystal* **A02**, 7–8 (1992).
50. K. Kawasaki, Y. Okano, S. Kan, M. Sakamoto, K. Hoshikawa, and T. Fukuda, "Uniformity of Fe-doped $LiNbO_3$ single crystal grown by the Czochralski method", *J. Crystal Growth* **119**, 317–321 (1992).
51. H.M. O'Bryan, P.K. Gallagher, and C.D. Brandle, "Congruent composition and Li-rich phase boundary of $LiNBO_3$", *J. Am. Ceram. Soc.* **68**, 493–496 (1985).
52. K. Nassau, H.J. Livingstein, and G.M. Loiacono, "Ferroelectric lithium niobate 1. growth, domain structure, dislocations and etching", *J. Phys. Chem. Solids* **27**, 983–988 (1966).
53. N. Niizeki, T. Yamada, and H. Toyoda, "Growth ridges, etched hillocks, and crystal structure of lithium niobate", *Jap. J. Appl. Phys.* **6**, 318–327 (1967).
54. Y.S. Luh, R.S. Feigelson, M.M. Fejer, and R.L. Byer, "Ferroelectric domain structures in $LiNbO_3$ single-crystal fibers", *J. Crystal Growth* **78**, 135–143 (1986).
55. B.K. Vainshtein, V.M. Fridkin, and V.L. Indenbom, "Structure of crystals", in *Modern Crystallography*, Springer Series in Solid-State Sciences", Vol. 21 Springer, Berlin, 1982.
56. S.V. Tsivinsky, "Factors governing dislocation density in Czochralski method of growing crystals", *Fiz. Metallov Metalloved.* **25**, 55–63 (1968).
57. S. Arahira, K. Watanabe, K. Shinozaki, and Y. Ogawa, "Successive excited-state absorption through a multistep process in highly Er^{3+}-doped fiber pumped by a 1.48 μm laser diode", *Opt. Lett.* **17**, 1679–1681 (1992).
58. J. Thogersen, N. Bjerre and J. Mark, "Multiphoton absorption and cooperative upconversion excitation in Er^{3+}-doped fibers," *Opt. Lett,* **13**, 197–199 (1993).
59. R. L. Laming, S.B. Poole, and E.J. Tarbox, "Pump excited-state absorption in erbium-doped fibers", *Opt. Lett.* **13**, 1084–1086 (1988).
60. J.F. Massicott, M.C. Brierley, R. Wyatt, S.T. Davey, and D. Szebesta, "Low threshold, diode pumped operation of a green, Er^{3+} doped fluoride fibre laser", *Electron Lett.* **29**, 2119–2120 (1993).
61. J.Y. Allain, M. Monerie, and H. Poignant, "Tunable green upconversion erbium fibre laser", *Electron Lett.* **28**, 111–113 (1992).
62. T.J. Whitley, C.A. Millar, R. Wyatt, M.C. Brierly, and D. Szebesta, "Upconversion pumped green lasing in erbium doped fluorozirconate fibre", *Electron Lett.* **27**, 1785–1786 (1991).
63. M. Fleuster, Ch. Buchal, E. Snoeks, and A. Ploman, "Rapid thermal annealing of MeV erbium implanted $LiNbO_3$ single crystals for optical doping", *J. Appl. Phys.* **75**, 225–227 (1994).
64. M. Tsuda, K. Inoue, S. Inoue, and A. Makishima, "Upconversion mechanism in Er^{3+}-doped fluorozirconate glasses under 800-nm excitation", *J. Appl. Phys.* **85**, 29–37 (1999).
65. J.W. Shur, W.S. Yang, S.J. Suh, J.H. Lee, T. Fukuda, and D.H. Yoon, "Growth and characterization of Er-doped stoichiometric $LiNbO_3$ single crystal fibers by the micro-pulling down method", *J. Crystal Growth* **229**, 223–227 (2001).
66. J.W. Shur, W.S. Yang, S.J. Suh, J.H. Lee, T. Fukuda, and D.H. Yoon, "Optical properties of Er doped congruent and stoichiometric $LiNbO_3$ single crystals", *Cryst. Res. Technol.* **37**, 353–358 (2002).
67. J. Amin, B. Dussardier, T. Schweizer, and M. Hempstead, "Spectroscopic analysis of Er^{3+} transitions in lithium niobate", *J. Lumin.* **69**, 17–26 (1996).
68. G. Zhong, J. Jia, and Z. Wu, *Proc. 11th International Quantum Electronics Conference*, *IEEE Catalogue* No. 80CH 1561-0, p. 631.
69. J.W. Shur, W.N. Jeon, S.M. Lee, W.S. Yang, H.Y. Lee, and D.H. Yoon, "Up-conversion property of Er_2O_3 and MgO co-doped stoichiometric $LiNbO_3$ single crystal by using the μ-PD method", *J. Kor. Ceram. Soc.* **39**, 835–839 (2002).
70. W.S. Yang, S.J. Suh, J.H. Lee, T. Fukuda, and D.H. Yoon, "Growth and upconversion properties of erbium doped $LiNbO_3$ single crystal fibers", *J. Kor. Asso. Crystal Growth* **9**, 377–380 (1999).
71. L.E. Myers, R.C. Eckardt, M.M. Fejer, R.L. Byer, W.R. Bosenberg, and J.W. Pierce, "Quasi-phase-matched optical parametric oscillators in bulk periodically poled $LiNbO_3$", *J. Opt. Soc. Am.* **B12**, 2102–2117 (1995).
72. W.S. Yang, J.H. Lee, T. Fukuda, and D.H. Yoon, "Micro-pulling down growth of Co-doped lithium niobate single crystal fibers according Er and Mg contents and

photolumenescence properties", *Cryst. Res. Technol.* **36**, 519–525 (2001).
73. Y. Waku, N. Nakagawa, T. Wakamoto, H. Ohtsubo, K. Shimizu, and Y. Kohtoku, "A ductile ceramic eutectic composite with high strength at 1.873 K", *Nature* **389**, 49–52 (1997).
74. T.A. Parthasarathy, T.Y. Mah, and L.E. Matson, "Deformation behaviour of an $Al_2O_3/Y_3Al_5O_{12}$ eutectic comparison with sapphire and YAG.", *J. Am. Ceram. Soc.* **76**, 29–32 (1993).
75. Y. Waku, H. Ohtsubo, N. Nakagawa, and Y. Koutoku, "Sapphire matrix composites reinforced with single crystal YAG phases", *J. Mater. Sci.* **31**, 4663–4670 (1996).
76. Y. Waku, N. Nakagawa, H. Ohtsubo, Y. Ohsora, and Y. Kohtoku, "High-temperature properties of unidirectionally solidified Al_2O_3/YAG composites", *J. Jap. Inst. Met.* **59**, 71–78 (1995).
77. Yoshikawa, B.M. Epelbaum, T. Fukuda, K. Suzuki, and Y. Waku, "Growth of $Al_2O_3/Y_3Al_5O_{12}$ eutectic fiber by micro-pulling-down method and its high-temperature strength and thermal stability", *Jap. J. Appl. Phys.* **38**, L55–L58 (1999).
78. F. Schmid and D. Viechnicki, "Oriented eutectic microstructures in system Al_2O_3/ZrO_2", *J. Mater. Sci.* **5**, 470–473 (1970).
79. S. Bourban, N. Karapatis, H. Hopmann, and W. Kurz, "Solidification microstructure of laser remelted Al_2O_3-ZrO_2 eutectic", *Acta Mater.* **45**, 5069–5075 (1997).
80. T. Ando and Y. Shiohara, "Metastable alumina structures in melt-extracted alumina-25 wt% zirconia and alumina-42 wt% zirconia ceramics", *J. Am. Ceram. Soc.* **74**, 410–417 (1991).
81. G.R. Fischer, L.J. Manfredo, R.N. MaNally, and R.C. Doman, "The eutectic and liquids in the Al_2O_3-ZrO_2 system", *J. Mater. Sci.* **16**, 3447–3451 (1981).
82. J. Echigoya, Y. Takabayashi, H. Suto, and M. Ishigame, "Structure and crystallography of directionally solidified Al_2O_3-ZrO_2 eutectic by the floating zone-melting method", *J. Mater. Sci. Lett.* **5**, 150–152 (1986).
83. J.H. Lee, A. Yoshikawa, S.D. Durbin, D.H. Yoon, T. Fukuda, and Y. Waku, "Microstructure of Al_2O_3/ZrO_2 eutectic fibers grown by the micro-pulling down method", *J. Crystal Growth* **222**, 791–796 (2001).
84. D.H. Yoon, I. Yonenaga, N. Onishi, and T. Fukuda, "Crystal growth of dislocation-free $LiNbO_3$ single crystals by micro pulling down method", *J. Crystal Growth* **142**, 339–343 (1994).
85. B.M. Epelbaum, A. Yoshikawa, K. Shimamura, T. Fukuda, K. Suzuki, and Y. Waku, "Microstructure of $Al_2O_3/Y_3Al_5O_{12}$ eutectic fibers grown by μ-PD method", *J. Crystal Growth* **198/199**, 471–475 (1999).
86. A. Yoshikawa, B.M. Epelbaum, K. Hasegawa, S.D. Durbin, and T. Fukuda, "Microstructures in oxide eutectic fibers grown by a modified micro-pulling-down method", *J. Crystal Growth* **205**, 305–316 (1999).
87. A. Yoshikawa, K. Hasegawa, J.H. Lee, S.D. Durbin, B.M. Epelbaum, D.H. Yoon, T. Fukuda, and Y. Waku, "Phase identification of $Al_2O_3/RE_3Al_5O_{12}$ and $Al_2O_3/REAlO_3$ (RE = Sm–Lu, Y) eutectics", *J. Crystal Growth* **218**, 67–73 (2000).
88. J.H. Lee, A. Yoshikawa, H. Kaiden, T. Fukuda, D.H. Yoon, and Y. Waku, "Growth and characterization of Al_2O_3-based $Y_3Al_5O_{12}$, ZrO_2 binary and ternary eutectic fibers", *J. Kor. Ass. Crystal Growth* **11**, 170–175 (2001).

